18. Allen, M. & Tildesley, D. *Computer Simulations of Liquids* (Clarendon, Oxford, 1990).
19. Stevens, M. *et al.* Comparison of shear flow hexadecane in a confined geometry and in bulk. *J. Chem. Phys.* **106,** 7303–7314 (1997).

Acknowledgements

This work was supported by an Institutional Grant from the Australian Research Council.

Correspondence and requests for materials should be addressed to P.H. (e-mail: peter@chem.usyd.edu.au).

High mixing rates in the abyssal Southern Ocean

Karen J. Heywood*, Alberto C. Naveira Garabato* & David P. Stevens†

* *School of Environmental Sciences,* † *School of Mathematics, University of East Anglia, Norwich NR4 7TJ, UK*

Mixing of water masses from the deep ocean to the layers above can be estimated from considerations of continuity in the global ocean overturning circulation[1–3]. But averaged over ocean basins, diffusivity has been observed to be too small[4–12] to account for the global upward flux of water, and high mixing intensities have only been found in the restricted areas close to sills and narrow gaps[10,11,13–15]. Here we present observations from the Scotia Sea, a deep ocean basin between the Antarctic peninsula and the tip of South America, showing a high intensity of mixing that is unprecedented over such a large area. Using a budget calculation over the whole basin, we find a diffusivity of $(39 \pm 10) \times 10^4$ m^2 s^{-1}, averaged over an area of 7×10^5 km^2. The Scotia Sea is a basin with a rough topography[16], situated just east of the Drake passage where the strong flow of the Antarctic Circumpolar Current is constricted in width. The high basin-wide mixing intensity in this area of the Southern Ocean may help resolve the question of where the abyssal water masses are mixed towards the surface.

Diapycnal eddy diffusivity K is a fundamental property of ocean flows, where turbulence and mixing dominate over molecular-scale diffusion. It quantifies the exchange of heat, salt and other tracers. Model evidence suggests that the value of K determines the strength of the overturning circulation[17,18] that controls the climate over much of the Earth. Yet the value of K is still remarkably unbounded over orders of magnitude[3]. An order of magnitude of 10^{-4} m^2 s^{-1} for the globally averaged value of K has been obtained by estimating that approximately 25 Sv (1 Sv $= 10^6$ m^3 s^{-1}) of cold, dense abyssal water forms in polar regions, and by assuming for simplicity that it upwells uniformly elsewhere into the thermocline[1,2]. More sophisticated versions of this calculation using inverse techniques and continent-to-continent hydrographic sections reveal basin-averaged diffusivities of similar magnitude, ranging from $(3–4) \times 10^{-4}$ m^2 s^{-1} for mid-depths to $(9–12) \times 10^{-4}$ m^2 s^{-1} for bottom layers[19]. Yet direct measurements suggest that K in most regions of the world

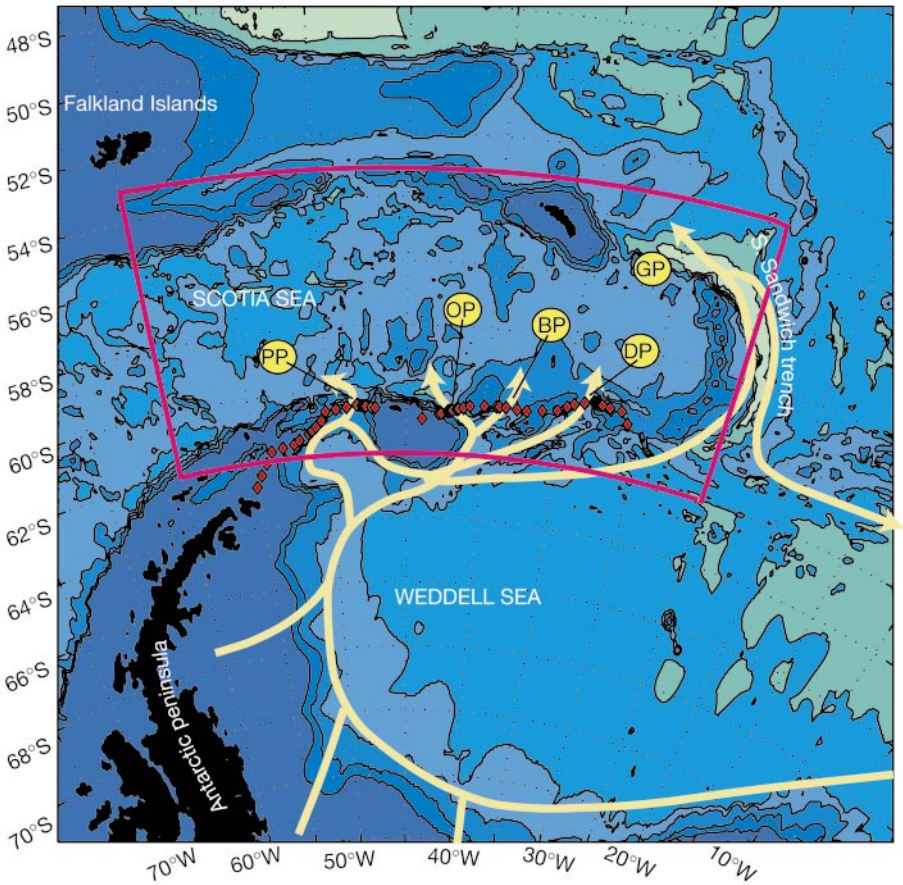

Figure 1 Map of the Scotia Sea, showing ALBATROSS stations (red diamonds) along the South Scotia Ridge. Bathymetric contours are shown every 1,000 m. Land is shaded black. Schematic pathways of Weddell Sea Deep Water (WSDW) are shown (yellow lines). Important passages through bathymetric constraints are marked: Georgia passage (GP) through the northern boundary of the Scotia Sea, and Phillip passage (PP), Orkney passage (OP), Bruce passage (BP) and Discovery passage (DP) through the South Scotia Ridge. The pink box marks the area shown in Fig. 2.

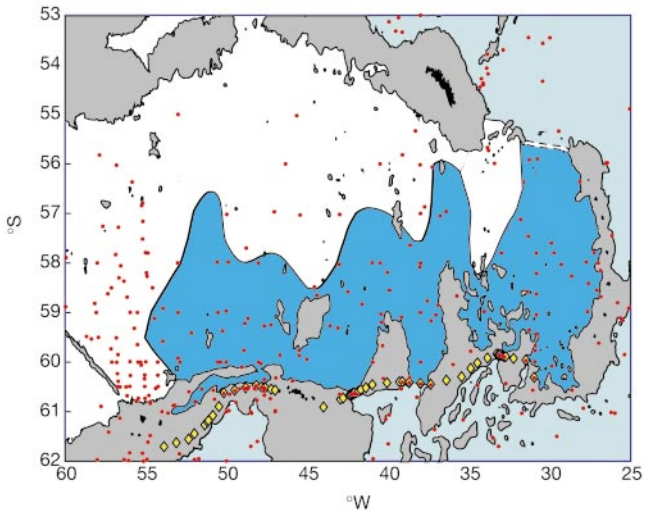

Figure 2 Map of the extent of the $\gamma^n = 28.31\,kg\,m^{-3}$ neutral density surface, shaded blue and light green. The blue area shows the closed area considered for the calculation of diffusivity. Red dots denote locations of all available historical hydrographic stations that contain WSDW. ALBATROSS stations (yellow diamonds) are shown along the South Scotia Ridge. Depths shallower than 2,000 m are shaded grey; land is shaded black. The dashed lines in the Georgia passage indicate the absence of LWSDW at the sill.

ocean is an order of magnitude less than this[4]. Recently it has been argued[20] that wind-driven upwelling in the Southern Ocean reduces the requirement for global average diapycnal eddy diffusivity to $3 \times 10^{-5}\,m^2\,s^{-1}$. However, this still demands some regions of substantially higher diffusivity.

The ALBATROSS (Antarctic large-scale box analysis and the role of the Scotia Sea) project[21] was designed to quantify the flow of water into and out of the Scotia Sea, particularly the deep, dense water that is formed in the Weddell Sea and provides the cold layers at the bottom of much of the world ocean. A quasi-synoptic box of densely spaced stations measuring temperature, salinity and current velocity was completed around the Scotia Sea (Fig. 1), mostly along the crest of the ridges surrounding the abyssal basin. Here we focus on the stations along the top of the South Scotia Ridge. Weddell Sea Deep Water (WSDW), with potential temperatures between −0.7 and 0 °C and neutral density γ^n (ref. 22) between 28.40 and $28.26\,kg\,m^{-3}$, forms in the Weddell Sea and escapes to the north, either through gaps in the South Scotia Ridge, or along the South Sandwich trench and the deep abyssal plains to the east[23]. It is the densest water escaping the Weddell Sea, and forms part of what is known as Antarctic Bottom Water, as it pervades the world ocean.

From ALBATROSS, concurrent measurements of velocity and water properties are available across each of the deep sills through which deep water can escape the Weddell Sea into the Scotia Sea: the Orkney passage, Philip passage, Bruce passage and Discovery passage (Fig. 2). The densest waters in the bottom of the Scotia Sea emanate from the Weddell Sea through these gaps in the South Scotia Ridge[23]. The class of WSDW colder than −0.25 °C and denser than $\gamma^n = 28.31\,kg\,m^{-3}$ (known as Lower WSDW, LWSDW[24]) cannot escape the Scotia Sea, as it is too deep to flow through the Georgia passage and there are no other inflows or outflows for waters of these densities. Thus our starting point is that the water denser than $\gamma^n = 28.31\,kg\,m^{-3}$ has entered the basin through the deep gaps in the South Scotia Ridge, and can only escape through mixing with overlying waters. By undertaking a heat budget of this water, we can deduce K.

If the temperature in the deep ocean is in steady state, the upward advection of cold water must be balanced by a downward diffusive heat flux[1]. For a flow into an enclosed basin, the heat budget can be written as

$$\rho V C_p(\theta_u - \theta_i) = A\left(G - \rho C_p K \frac{\partial\theta}{\partial z}\right)$$

where ρ is the *in situ* density of sea water; V is the volume transport of water into the basin; C_p is the specific heat capacity of sea water; θ_i and θ_u are the potential temperatures of the inflowing water and of that upwelled through the upper surface; A is the area of the basin; G is the geothermal heat flux; K is the thermal diapycnal eddy diffusivity; and $\partial\theta/\partial z$ is the mean vertical gradient of potential temperature.

Values used for the calculation of K are summarized in Table 1, and their derivation discussed in the Methods section. Diapycnal

Table 1 Parameters used in the calculation of diapycnal eddy diffusivity *K*

	Heat budget	Salt budget
ρ, *in situ* density of sea water	$1{,}040\,kg\,m^{-3}$	Not required
V, volume transport of water into basin	4.0 ± 0.5 Sv*	4.0 ± 0.5 Sv
θ_i, or S_i, potential temperature or salinity of inflowing water	-0.438 ± 0.007 °C	34.654 ± 0.002
θ_u or S_u, potential temperature or salinity of water upwelled through upper surface	-0.250 ± 0.003 °C	34.663 ± 0.003
C_p, specific heat capacity of sea water	$3.91 \times 10^3\,J\,kg^{-1}\,°C^{-1}$	Not required
A, area of basin	$(7.0 \pm 1.0) \times 10^{11}\,m^2$	$(7.0 \pm 1.0) \times 10^{11}\,m^2$
G, geothermal heat flux	$0.1 \pm 0.1\,W\,m^{-2}$	Not required
$\frac{\partial\theta}{\partial z}$ or $\frac{\partial S}{\partial z}$, mean vertical gradient of potential temperature or salinity	$(2.7 \pm 0.3) \times 10^{-4}\,°C\,m^{-1}$	$(6.8 \pm 0.5) \times 10^{-6}\,m^{-1}$
K, diapycnal eddy diffusivity	$(39 \pm 10) \times 10^{-4}\,m^2\,s^{-1}$	$(79 \pm 45) \times 10^{-4}\,m^2\,s^{-1}$

See Methods for details of calculations.
* $1\,Sv = 10^6\,m^3\,s^{-1}$.

eddy diffusivity in the Scotia Sea is calculated to be 39×10^{-4} m^2 s^{-1}. Accounting for each of the error sources (Table 1), and assuming that they are independent, gives an uncertainty of 10×10^{-4} m^2 s^{-1}. A similar calculation can be made using a salinity budget (Table 1), yielding a value for K of $(79 \pm 45) \times 10^{-4}$ m^2 s^{-1}. We assume that there is no loss or gain of salt at the sea bed. The uncertainty in K is much larger because the difference between inflowing and upwelling salinity is small compared with the achievable precision of salinity measurements. That the two estimates of K are indistinguishable, within the uncertainties, indicates that the dominant process here is diapycnal mixing by fine-scale turbulence[9].

The vertical length scale L ($L = KA/V$) over which the upwelling water mixes is (680 ± 180) m. As recently pointed out[20], to close the global overturning circulation, the Antarctic Bottom Water need only be mixed to the depth of the deep waters sourced in the North Atlantic, and not to the sea surface. In the Scotia Sea, our data show that this mixing is indeed accomplished. The volume of LWDSW in the Scotia Sea is $(3.0 \pm 0.5) \times 10^{14}$ m^3, which implies a residence time of only (2.4 ± 0.5) years, a remarkably rapid flushing time.

Previous budget studies using similar calculations for other abyssal basins have not found such a high value as we have for the Scotia Sea. These include 4×10^{-4} m^2 s^{-1}, $(3.6–7.2) \times 10^{-4}$ m^2 s^{-1} and $(3 \pm 2) \times 10^{-4}$ m^2 s^{-1} averaged over the Brazil basin[6,9,12], $(1–4) \times 10^{-4}$ m^2 s^{-1} for North Atlantic abyssal basins[5,7] and $(10.6 \pm 2.7) \times 10^{-4}$ m^2 s^{-1} for the Somali basin in the Indian Ocean[8]. The Somali and Brazil basins are comparable in area to the Scotia Sea basin considered here. More recently, attention has been focused on regions in the close vicinity of sills and gaps through ridges. Direct measurements[13] of turbulent mixing of Antarctic Bottom Water in and just downstream of the Romanche fracture zone give K as high as 150×10^{-4} m^2 s^{-1}, suggesting that significant mixing occurs within narrow passages. Using similar methods to ours, in and just downstream of the Samoa passage diffusivities were determined of the order of $(50–500) \times 10^{-4}$ m^2 s^{-1} depending on the values taken for the vertical gradient of potential temperature[10]. Diffusivity in the southern central Indian basin averages $(35 \pm 14) \times 10^{-4}$ m^2 s^{-1}, ranging from 105×10^{-4} m^2 s^{-1} close to the sill in the Ninetyeast Ridge, and 13×10^{-4} m^2 s^{-1} away from the sill[11]. The area of our diffusivity calculation is more than an order of magnitude greater than the areas considered by each of these authors ($(2–3) \times 10^4$ km^2 compared with our area of 7×10^5 km^2). We note that the high value of K calculated here for the Scotia Sea is a basin average. The Scotia Sea is a region of rough bathymetry, but the value was not determined for a constricted passage.

The LWSDW exported to the Scotia Sea represents up to 38% of the total WSDW exported from the Weddell Sea[23]. If the Weddell Sea contributes 60–70% of all Antarctic Bottom Water production[25], defined as the global ocean waters denser than $\gamma^n = 28.27$ kg m^{-3}, then the LWSDW upwelling in the Scotia Sea represents up to 20% of all Antarctic Bottom Water production. This is a significant fraction of the water mass that cools the global ocean, and implies that ocean models that miss the exchange of waters between the Weddell and Scotia Sea—by not resolving the flow through the deep, narrow passages in the ridges around the Scotia Sea—will be unable to represent accurately the lower limb of the overturning circulation.

The Southern Ocean is generally weakly stratified, shown by the low value of Brunt-Väisälä frequency of $(5.4 \pm 0.2) \times 10^{-4}$ s^{-1} at the $\gamma^n = 28.31$ kg m^{-3} isopycnal in the Scotia Sea. A high value of diffusivity does not necessarily imply a large energy dissipation, if stratification is low. The dissipation we find is 1.1×10^{-9} W kg^{-1}, similar to, but slightly smaller than, values deduced for the deep Brazil basin[12]. Taking the median thickness of the LWDSW layer to be (423 ± 20) m, to mix the LWSDW into the overlying waters implies an energy dissipation of $(1.8 \pm 0.5) \times 10^9$ W: small in comparison with the global requirements of 2.1×10^{12} W (ref. 2) or 0.6×10^{12} W (ref. 20), and not disproportionate with the area over which the mixing is occurring.

Direct measurements of abyssal turbulence[14] indicate that mixing rates in the bulk of the ocean interior are at least an order of magnitude smaller than the basin-averaged budget-derived values. Enhanced diffusivity has been observed over steeply sloping boundaries and seamounts in the abyssal ocean: $K > 1 \times 10^{-4}$ m^2 s^{-1}, compared with values an order of magnitude smaller over smooth topography[4,14,15]. Our very large value for K suggests that the rough topography of the Scotia Sea plays a role in enhancing the mixing in this region. It is possible that the mechanism for this is the interaction of internal tides or other internal waves with topography[2,15], such as internal wave reflection occurring at sloping boundaries. Global maps of the energy estimated to be dissipated by tides[26,27] imply that the Scotia Sea may be a region where large amounts of energy are supplied to internal tides by the tidal flow of a stratified ocean over rough topography. Other possible sources for the energy are internal lee waves generated by interaction of the currents with the rough topography[28], and basin-trapped barotropic planetary wave modes[29].

The work that we report here leads us to believe that the Scotia Sea acts as a 'blender' to mix ocean water masses, and that *in situ* observations of turbulence in this region would confirm a significant contribution to the 'missing mixing' required to balance the global ocean overturning circulation. □

Methods

Inflow volume transport and inflow properties

LADCP (lowered acoustic Doppler current profiler) measurements throughout the water column provide a known level with which to reference geostrophic shear[23]. Bottom triangles below the deepest common depth of adjacent stations are included by extrapolating the deepest velocity value to the sea bed. An estimate of the uncertainty in the transport is provided from 1,000 calculations each applying a random baratropic perturbation to each LADCP profile, assuming a normal distribution with a standard deviation of 3 cm s^{-1}. This assumes that the dominant source of error is the barotropic component deduced from the LADCP, and that the errors are horizontally uncorrelated. We determine the net inflow of water denser than $\gamma^n = 28.31$ kg m^{-3} and the associated mean volume-transport-weighted temperature and salinity of this water from the direct ALBATROSS measurements. The volume transport of 4 Sv is consistent with heat and mass budgets of the Weddell gyre[23].

Outflow area, outflow properties and property gradients

The outflow potential temperature and salinity across the $\gamma^n = 28.31$ kg m^{-3} isopycnal, the area of this isopycnic surface, and the vertical gradients of potential temperature and salinity in the WSDW layer in the Scotia Sea, were calculated using climatological deep hydrographic stations. The Hydrographic Atlas of the Southern Ocean (HASO) database[30] was used as the primary source of quality controlled hydrographic data within the Scotia Sea basin. ALBATROSS stations and the 1993 crossing of the World Ocean Circulation Experiment (WOCE) Drake passage repeat section SR1b[24] were added at the standard HASO vertical grid spacing, typically 500 m at the depths of the $\gamma^n = 28.31$ kg m^{-3} isopycnal. Comparison with a detailed bathymetric data set[16] excluded all stations that did not extend to within 250 m of the sea bed or were in water depths shallower than 1,000 m.

To determine the area of the $\gamma^n = 28.31$ kg m^{-3} isopycnal, we selected all stations with bottom neutral density greater than or equal to 28.26 kg m^{-3}, thus including all types of WSDW. This yields 299 stations. The bottom neutral densities were gridded on a $0.5° \times 0.5°$ grid, with a search radius of 200 km and smoothing the influence of each point over 50 km (Fig. 2). Experimentation with various gridding options gave an estimate of the uncertainty of 1.0×10^{11} m^2, including consideration of the sparsity of the data.

Eighty-three individual hydrographic stations sampled water as dense or denser than $\gamma^n = 28.31$ kg m^{-3} in the Scotia Sea (Fig. 2). The potential temperature and salinity on this isopycnal were determined for each station, and the median value selected to minimize the effect of outliers. The outflow potential temperature was −0.25 °C, as we would expect, as the −0.25 °C isotherm is often chosen as the indicator of the boundary of LWSDW. We allocate this a small uncertainty (±0.003 °C); in the calculation of diffusivity the pertinent quantity is the difference between the inflow and outflow temperatures, θ_i minus θ_u, to which we allocate a combined uncertainty of ±0.01 °C. For comparison, the salinity difference is 0.009 with an estimated uncertainty of 0.005, indicating the greater robustness of the heat budget calculation.

The same stations provided an estimate of the vertical gradient of potential temperature and salinity at the depth of the $\gamma^n = 28.31$ kg m^{-3} isopycnal. This is one of the least well defined quantities in the heat budget calculation, because of poor vertical and horizontal data density. If we grid the same 83 stations and produce an area-weighted mean, the

difference in the resulting $\partial\theta/\partial z$ is 0.2×10^{-4} °C m^{-1}. Taking this as the uncertainty in $\partial\theta/\partial z$, together with the uncertainty caused by the relatively small number of stations, we allocate an uncertainty of 0.3×10^{-4} °C m^{-1}. The vertical salinity gradient at this isopycnal was 6.8×10^{-6} m^{-1} with an estimated uncertainty of 0.5×10^{-6} m^{-1}.

Geothermal heating

In some regions of the sea floor, geothermal heating is negligible. Flow through the oceanic crust is a function of the age of the crust; younger crust provides greater heating. The Scotia Sea exhibits a wide variety of ages. We estimate a typical value for G to be 0.1 W m^{-2}, and use this in the heat budget equation with an uncertainty of 0.1 W m^{-2}.

Seawater density, specific heat capacity

For the situation where geothermal heating is included, values for the *in situ* density of sea water and the specific heat capacity are required. We used the HASO climatological data set to determine representative median values. The uncertainty in these is negligible compared with other uncertainties in the calculation.

Received 9 October; accepted 19 December 2001.

1. Munk, W. H. Abyssal recipes. *Deep-Sea Res.* **13,** 207–230 (1966).
2. Munk, W. H. & Wunsch, C. Abyssal recipes II: energetics of tidal and wind mixing. *Deep-Sea Res. I* **45,** 1997–2010 (1998).
3. Toole, J. M. & McDougall, T. J. in *Ocean Circulation and Climate* (eds Siedler, G., Church, J. & Gould, J.) 337–355 (Academic, London, 2001).
4. Toole, J. M., Polzin, K. L. & Schmitt, R. W. Estimates of diapycnal mixing in the abyssal ocean. *Science* **264,** 1120–1123 (1994).
5. Whitehead, J. A. & Worthington, L. V. The flux and mixing rates of Antarctic Bottom Water within the North Atlantic. *J. Geophys. Res.* **87,** 7903–7924 (1982).
6. Hogg, N. G., Biscaye, P., Gardner, W. & Schmitz, W. J. On the transport and modification of Antarctic Bottom water in the Vema Channel. *J. Mar. Res.* **40** (suppl.), 231–263 (1982).
7. Saunders, P. M. Flow through Discovery gap. *J. Phys. Oceanogr.* **17,** 631–643 (1987).
8. Barton, E. D. & Hill, A. E. Abyssal flow through the Amirante Trench (Western Indian Ocean). *Deep-Sea Res. A* **36,** 1121–1126 (1989).
9. Durrieu de Madron, X. & Weatherly, G. Circulation, transport and bottom boundary layers of the deep currents in the Brazil Basin. *J. Mar. Res.* **52,** 583–638 (1994).
10. Roemmich, D., Huatala, S. & Rudnick, D. Northward abyssal transport through the Samoan Passage and adjacent regions. *J. Geophys. Res.* **101,** 14039–14055 (1996).
11. McCarthy, M. C., Talley, L. D. & Baringer, M. O. Deep upwelling and diffusivity in the southern Central Indian Basin. *Geophys. Res. Lett.* **24,** 2801–2804 (1997).
12. Morris, M. Y., Hall, M. M., St Laurent, L. C. & Hogg, N. G. Abyssal mixing in the Brazil Basin. *J. Phys. Oceanogr.* **31,** 3331–3348 (2001).
13. Polzin, K. L., Speer, K. G., Toole, J. M. & Schmitt, R. W. Intense mixing of Antarctic Bottom Water in the equatorial Atlantic Ocean. *Nature* **380,** 54–57 (1996).
14. Polzin, K. L., Toole, J. M., Ledwell, J. R. & Schmitt, R. W. Spatial variability of turbulent mixing in the abyssal ocean. *Science* **276,** 93–96 (1997).
15. Ledwell, J. R. *et al.* Evidence for enhanced mixing over rough topography in the abyssal ocean. *Nature* **403,** 179–182 (2000).
16. Smith, W. H. F. & Sandwell, D. T. Global sea floor topography from satellite altimetry nd ship depth soundings. *Science* **277,** 1956–1962 (1997).
17. Huang, R. X. Mixing and energetics of the oceanic thermohaline circulation. *J. Phys. Oceanogr.* **29,** 727–746 (1999).
18. Zhang, J., Schmitt, R. W. & Huang, R. X. The relative influence of diapycnal mixing and hydrologic forcing on the stability of the thermohaline circulation. *J. Phys. Oceanogr.* **29,** 1096–1108 (1999).
19. Ganachaud, A. & Wunsch, C. Improved estimates of global ocean circulation, heat transport and mixing from hydrographic data. *Nature* **408,** 453–457 (2000).
20. Webb, D. J. & Suginobara, N. Vertical mixing in the ocean. *Nature* **409,** 37 (2001).
21. Naveira Garabato, A. C., Heywood, K. J. & Stevens, D. P. Modification and pathways of Southern Ocean deep waters in the Scotia Sea. *Deep-Sea Res. I* (in the press).
22. Jackett, D. R. & McDougall, T. J. A neutral density variable for the world's oceans. *J. Phys. Oceanogr.* **27,** 237–263 (1997).
23. Naveira Garabato, A. C., McDonagh, E. L., Stevens, D. P., Heywood, K. J. & Sanders, R. J. On the export of Antarctic Bottom Water from the Weddell Sea. *Deep-Sea Res. II* (2002).
24. Arhan, M., Heywood, K. J. & King, B. A. The deep waters from the Southern Ocean at the entry to the Argentine Basin. *Deep-Sea Res. II* **46,** 475–499 (1999).
25. Orsi, A. H., Johnson, G. C. & Bullister, J. L. Circulation, mixing and production of Antarctic Bottom Water. *Prog. Oceanogr.* **43,** 55–109 (1999).
26. Egbert, G. D. & Ray, R. D. Significant dissipation of tidal energy in the deep ocean inferred from satellite altimeter data. *Nature* **405,** 775–778 (2000).
27. Sjoberg, B. & Stigebrandt, A. Computations of the geographical distribution of the energy flux to mixing processes via internal tide and the associated vertical circulation in the ocean. *Deep-Sea Res.* **39,** 269–291 (1992).
28. Bell, T. H. Topographically-generated internal waves in the open ocean. *J. Geophys. Res.* **80,** 320–327 (1975).
29. Fukumori, I., Raghunath, R. & Fu, L.-L. Nature of global large-scale sea level variability in relation to atmospheric forcing: a modelling study. *J. Geophys. Res.* **103,** 5493–5512 (1998).
30. Olbers, D., Gouretski, V., Seiss, G. & Schroter, J. *Hydrographic Atlas of the Southern Ocean* (Alfred Wegener Inst. for Polar and Marine Res., Bremerhaven, Germany, 1992).

Acknowledgements

We thank P. Barker and F. Vine for discussions regarding the magnitude of geothermal heating in the Scotia Sea. ALBATROSS was funded by the Natural Environment Research Council.

Competing interests statement

The authors declare that they have no competing financial interests.

Correspondence and requests for information should be addressed to K.J.H. (e-mail: k.heywood@uea.ac.uk).

Sudden aseismic fault slip on the south flank of Kilauea volcano

Peter Cervelli*†, Paul Segall*, Kaj Johnson*, Michael Lisowski‡ & Asta Miklius†

* *Department of Geophysics, Mitchell Building, Stanford University, Stanford, California 94305-2215, USA*
† *US Geological Survey, Hawaiian Volcano Observatory, Hawaii National Park, Hawaii 96718, USA*
‡ *US Geological Survey, Cascades Volcano Observatory, 5400 MacArthur Blvd, Vancouver, Washington 98661, USA*

One of the greatest hazards associated with oceanic volcanoes is not volcanic in nature, but lies with the potential for catastrophic flank failure[1,2]. Such flank failure can result in devastating tsunamis and threaten not only the immediate vicinity, but coastal cities along the entire rim of an ocean basin[3]. Kilauea volcano on the island of Hawaii, USA, is a potential source of such flank failures[3,4] and has therefore been monitored by a network of continuously recording geodetic instruments, including global positioning system (GPS) receivers, tilt meters and strain meters. Here we report that, in early November 2000, this network recorded transient southeastward displacements, which we interpret as an episode of aseismic fault slip. The duration of the event was about 36 hours, it had an equivalent moment magnitude of 5.7 and a maximum slip velocity of about 6 cm per day. Inversion of the GPS data reveals a shallow-dipping thrust fault at a depth of 4.5 km that we interpret as the down-dip extension of the Hilina Pali–Holei Pali normal fault system. This demonstrates that continuously recording geodetic networks can detect accelerating slip, potentially leading to warnings of volcanic flank collapse.

Data from the Kilauea GPS network (Fig. 1) are routinely analysed in 24-h batches at the US Geological Survey's Hawaiian Volcano Observatory (HVO). Figure 2 depicts the time series of selected stations on Kilauea's south flank as well as of three more distant stations. The south flank stations show clear offsets of up to 15 mm in early November, while the remote sites do not. The estimated displacements between 8 November and 10 November determined from the daily solutions are shown in Fig. 1. The spatial coherence of the signal and the negligible displacements far from the south flank (Fig. 1) rule out the possibility that the displacements are an artefact of unmodelled errors in the GPS time series.

We interpret the deformation field as resulting from fault slip. The data cannot be fitted by a dyke, sill, or expanding magma chamber. Moreover, there is no evidence of summit deflation, which usually accompanies magmatic activity. Nonlinear optimization[5] of the observed displacements for the best-fitting fault geometry yields a thrust, which dips shallowly ($4° \pm 10°$, uncertainties estimated using a bootstrap method[6]) toward the volcano (Figs 1 and 3). The average slip on the fault is 87 mm. The model-predicted displacements fit the observations, including the vertical components (Figs 1 and 3), extremely well (normalized mean square error of 1.2). The largest south flank earthquake during the first two weeks of November was a magnitude 2.7, which occurred on 3 November (Fig. 1). Thus, this event can be placed among the class of 'silent' earthquakes, which have been recently detected by large-scale